Thermochimica Acta 490 (2009) 51–59

Contents lists available at ScienceDirect

Thermochimica Acta

journal homepage: www.elsevier.com/locate/tca

Comparative evolved gas analytical and structural study on *trans*-diammine-bis(nitrito)-palladium(II) and platinum(II) by TG/DTA–MS, TG–FTIR, and single crystal X-ray diffraction

János Madarász[a,*], Petra Bombicz[b], Czugler Mátyás[b], Ferenc Réti[c], Gábor Kiss[c], György Pokol[a]

[a] Department of Inorganic and Analytical Chemistry, Budapest University of Technology and Economics, Szt. Gellért tér 4, Budapest H-1521, Hungary
[b] Institute of Structural Chemistry, Chemical Research Center, Hungarian Academy of Sciences, Budapest H-1525, POB 17, Hungary
[c] Department of Atomic Physics, Budapest University of Technology and Economics, Budafoki út 8, Budapest H-1111, Hungary

ARTICLE INFO

Article history:
Received 3 December 2008
Received in revised form 2 February 2009
Accepted 6 February 2009
Available online 21 February 2009

Keywords:
Evolved gas analysis (EGA)
Mass spectrometry (MS)
FTIR-spectroscopic gas cell
Simultaneous thermogravimetry (TG) and differential thermal analysis (DTA)
Single crystal X-ray diffraction
Determination of molecular and crystal structure
CO sensors
Pt and Pd catalysts

ABSTRACT

Detailed study on identification and thermal decomposition of solid title compounds **1** and **2** crystallized from the used aqueous ammonia solutions of $Pd(NH_3)_2(NO_2)_2$ and $Pt(NH_3)_2(NO_2)_2$, has been carried out. Beyond the composition of complexes **1** and **2**, their *trans* square planar configuration have already been recognized by reference IR spectra and powder XRD patterns, nevertheless their exact molecular and crystal structure as of *trans*-$Pd(NH_3)_2(NO_2)_2$ (**1**, Pd-NN) and *trans*-$Pt(NH_3)_2(NO_2)_2$ (**2**, Pt-NN) has been determined by single crystal X-ray diffraction ($R = 0.0515$ and 0.0341), respectively. Despite their compositional and configuration analogy, they crystallize in different crystal systems and space groups. The crystals of **1** (Pd-NN) are triclinic (space group No. 2, *P*-1, $a = 5.003(1)$ Å, $b = 5.419(1)$ Å, $c = 6.317(1)$ Å, $\alpha = 91.34(2)^\circ$, $\beta = 111.890(10)^\circ$, $\gamma = 100.380(10)^\circ$), while those of **2** (Pt-NN) are monoclinic (space group No. 5, *C*2, $a = 7.4235(16)$ Å, $b = 9.130(2)$ Å, $c = 4.4847(10)$ Å, $\beta = 99.405(7)^\circ$).

The pyrolytic processes of **1** and **2** (which might be sensitive to shock and heat) have been followed by simultaneous thermogravimetric and differential thermal analysis (TG/DTA), while the evolved gaseous species have been traced *in situ* by online coupled TG/DTA–EGA–MS and TG–EGA–FTIR instruments in He and air. Pd and Pt powders, forming as final solid products in single step, are captured and checked by TG and XRD. Whilst the unified evolved gas analyses report evolution of N_2, H_2O, NH_3, N_2O, NO, and NO_2 gases as gaseous product components in the exothermic decomposition of both *trans*-$Pd(NH_3)_2(NO_2)_2$ (**1**) and *trans*-$Pt(NH_3)_2(NO_2)_2$ (**2**) starting from ca. 230 and 220 °C, in sealed crucibles with a pinhole on the top, respectively.

1. Introduction

This study has been directly initiated by the work of Kiss et al. [1], who studied the CO sensitivity of SnO_2 thick layer sensors impregnated with $Pt(NH_3)_2(NO_2)_2$ and $Pd(NH_3)_2(NO_2)_2$ depending on their fabrication temperature. The complexes had been decomposed by heat treatments in range of 150–350 °C in air, and the surface composition had achieved were evaluated by X-ray photoelectron spectroscopy (XPS) [1]. Basically PtO and PdO was found to be present on the surface beyond some $Pt(OH)_2$ and some partially decomposed Pd complex, respectively [1]. Despite these spurious XPS findings, starting with commercially available aqueous ammonia solutions of $Pd(NH_3)_2(NO_2)_2$ and $Pt(NH_3)_2(NO_2)_2$, after impregnations and heat treatments between 150 and 350 °C, a successful sensitization of SnO_2 layers for CO gas has been observed at 90 °C [1].

In order to get a deeper insight in to chemical mechanism of the sensitization process, we have tried to identify the active sensing chemical species of residues obtainable from the impregnating Pd or Pt solutions, on a higher mass scale and with other analytical methods different from XPS. We could carry out a detailed study on thermal decomposition of solid *trans*-$Pd(NH_3)_2(NO_2)_2$ (**1**, Pd-NN) and *trans*-$Pt(NH_3)_2(NO_2)_2$ (**2**, Pt-NN), which actually firstly crystallized from the applied commercial aqueous ammoniacal solutions. Both solid and gaseous state analyses of the decomposition products have been performed by powder XRD and evolved gas analysis (EGA), respectively.

The essentially violent thermal decomposition processes of solid complexes **1** and **2** has been studied and followed by simultaneous thermogravimetric (TG) and differential thermal analysis (TG/DTA) in semi-sealed Al crucibles, while the evolved gaseous species has been traced *in situ* by online coupled TG/DTA–EGA–MS and TG–EGA–FTIR instruments in He and air, whilst the solid residues

* Corresponding author. Tel.: +361 463 4047; fax: +361 463 3408.
E-mail address: madarasz@mail.bme.hu (J. Madarász).

0040-6031/$ – see front matter © 2009 Elsevier B.V. All rights reserved.
doi:10.1016/j.tca.2009.02.006

Table 1
Crystal data, data collection and structure refinement of compounds *trans*-$Pd(NH_3)_2(NO_2)_2$ (**1**, Pd-NN) and *trans*-$Pt(NH_3)_2(NO_2)_2$ (**2**, Pt-NN).

	1 *trans*-$Pd(NH_3)_2(NO_2)_2$	**2** *trans*-$Pt(NH_3)_2(NO_2)_2$
Empirical formula	$PdN_4H_6O_4$	$PtN_4H_6O_4$
Formula weight	232.49	321.17
Temperature (K)	293(2)	295(2)
Radiation wave length, λ (Å),	0.710730, (MoK()	0.710730 (MoK()
Crystal system	Trilinic	Monoclinic
Space group	*P*-1, No. 2	*C*2, No. 5
Unit cell dimensions		
a (Å)	5.003(1)	7.4235(16)
b (Å)	5.419(1)	9.130(2)
c (Å)	6.317(1)	4.4847(10)
α (°)	91.34(2)	90
β (°)	111.89(1)	99.405(7)
γ (°)	100.38(1)	90
Volume (Å^3)	155.54(5)	299.87(11)
Z/Z'	1/0.5	2/0.5
Density (calculated) [Mg m^{-3}]	2.482	3.557
Absorption coefficient, μ (mm^{-1})	2.939	23.352
F(0 0 0)	112	288
Crystal colour	Bright yellow	Colourless
Crystal description	Block	Block
Crystal size (mm)	0.30 × 0.20 × 0.10	0.13 × 0.33 × 0.41
Absorption correction	Semi-empirical (ψ-scan)	Numerical
Max. and min. transmission	1.000 and 0.505	1.000 and 0.8977
θ range for data collection (°)	$3.49 \le \theta \le 24.99$	$3.6 \le \theta \le 27.5$
Index ranges	$-10 \le h \le 10$;	$-9 \le h \le 9$;
	$-11 \le k \le 11$;	$-11 \le k \le 11$;
	$-13 \le l \le 13$	$-5 \le l \le 5$
Reflections collected	7134	1706
Completeness to 2θ	0.998	0.932
Independent reflections	3262 [R(int) = 0.0345]	673 [R(int) = 0.072]
Reflections $I > 2\sigma$(I)	2618	673
Data/restraints/parameters	3262/0/46	673/0/45
Goodness-of-fit on F^2	1.510	1.13
Final R indices ($I > 2\sigma(I)$)		
R1	0.0515	0.0341
R2	0.1002	0.0788
R indices (all data)		
R1	0.0875	0.0341
R2	0.1235	0.0788
Extinction coefficient	0.097(8)	0.0053(7)
Max. and mean shift/esd	0.000, 0.000	0.008, 0.001
Largest diff. peak and hole (e A^{-3})	2.629 and −3.197	0.99 and −2.86

The weighting schemes applied for **1** and **2** respectively was 1. $w = 1/[\sigma^2(F_0^2) + (0.0202P)^2 + 0.3178P]$ where $P = (F_0^2 + 2F_c^2)/3$. and 2. $w = 1/[\sigma^2(F_0^2) + (0.0563P)^2 + 0.0P]$ where $P = (F_0^2 + 2F_c^2)/3$.

Table 2
Comparison of the FTIR spectra segments in ref [11] and the present work.

Band positions (cm^{-1}) for *trans*-$Pd(NH_3)_2(NO_2)_2$		Band positions (cm^{-1}) for *trans*-$Pt(NH_3)_2(NO_2)_2$	
In ref. [11]	In present work	In ref. [11]	In present work
1375	1386	1365	1370
1325	1327	1325	1334
1255	1261	1282	1288
830	828	828	829
800	791	–	–
588	592	626	628
494	496	518	524

Table 3
Intermolecular interactions in the complexes of **1** (Pd-NN) and **2** (Pt-NN).

1 (Pd-NN)	d(D–H) (Å)	d(H···A) (Å)	d(D···A) (Å)	ψ(D–H···A) (°)	Symmetry operation
N1-H11···O32	0.89	2.15	3.034(5)	170	$x,1+y,z$
N1-H12···O32	0.89	2.21	3.085(5)	168	$1+x,1+y,z$
N1-H13···O31	0.89	2.26	3.136(5)	169	$1-x,-y,1-z$
2 (Pt-NN)	d(D–H) (Å)	d(H···A) (Å)	d(D···A) (Å)	ψ(D–H···A) (°)	Symmetry operation
N1-H11···O21	0.89	2.33	2.89(4)	121	Intra
N1-H12···O31	0.89	2.34	2.81(4)	113	Intra
N1-H11···O31	0.89	2.34	3.14(3)	150	$1/2-x,-1/2+y,1-z$
N1-H12···O21	0.89	2.26	3.05(4)	147	$1/2-x,1/2+y,1-z$
N1-H13···O21	0.89	2.50	3.21(4)	137	$1/2-x,1/2+y,-z$

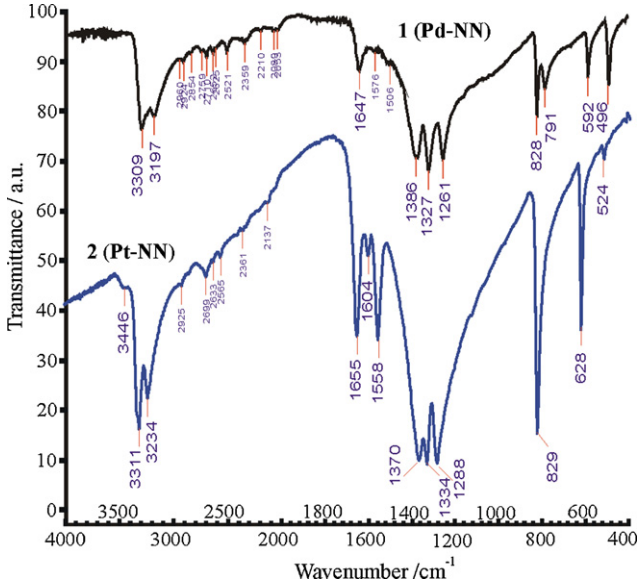

Fig. 1. FTIR spectra of samples **1** (Pd-NN) and **2** (Pt-NN) in KBr.

are checked by XRD phase analysis. Especially a better understanding of mechanism and dynamics of the gas evolution from these solid complexes **1** and **2** which are probably sensitive also to shock, seems to be essential during a scaling up of the sensor fabrication.

2. Experimental

2.1. Samples and methods

The samples **1** and **2** were crystallized at room temperature by slow evaporation of the solvent then filtered from commercially available precursor solutions of the Aldrich Chem. Co. with PN 33,990-3 ('Diamminedinitritopalladium(II) solution in dilute ammonium hydroxide, Pd cc. 5%. Dry material may be shock sensitive! Protect from light'!) and PN 33,988-1 (diammine dinitritoplatinum(II) 3.4 wt% solution in dilute ammonium hydroxide, Light sensitive! Dry material may be shock sensitive!), which were used as received.

FTIR spectra of solid samples **1** and **2** were measured by Excalibur Series FTS 3000 (BioRad) FTIR spectrophotometer in KBr (with gentle powdering and suitable precautions) between 400 and 4000 cm^{-1}, meanwhile the XRD patterns of theirs and their solid decomposition products obtained after the thermal runs from the thermal balances were recorded on X'pert Pro MPD (PANalytical Bv, The Netherlands) X-ray diffractometer using Cu Kα radiation with Ni filter and X'celerator detector.

2.2. Structure determination and refinement by single crystal X-ray diffraction of trans-$Pd(NH_3)_2(NO_2)_2$ (**1**) and trans-$Pt(NH_3)_2(NO_2)_2$ (**2**)

A bright yellow single crystal of **1** was mounted on glass fiber. Cell parameters were determined by least-squares of the setting angles of 25 reflections ($18.37^\circ \leq \theta \leq 19.58^\circ$). Intensity data with ω–2θ scans were collected on an Enraf-Nonius CAD4 diffractometer using graphite monochromated MoKα radiation. Data reductions was carried out by program XCAD4 [2], while the empirical absorption corrections were done by MolEN [3]. The scan width was $0.61 + 0.82\mathrm{tg}(\theta)^\circ$ in ω. Backgrounds were measured 1/2 the total time of the peak scans. The intensities of three standard reflections were monitored every 60 min. The intensities of the standard reflections indicated a crystal decay of 1%, the data were corrected for decay, R(sigma) = 0.0359]. Completeness to $2\theta = 0.998^\circ$.

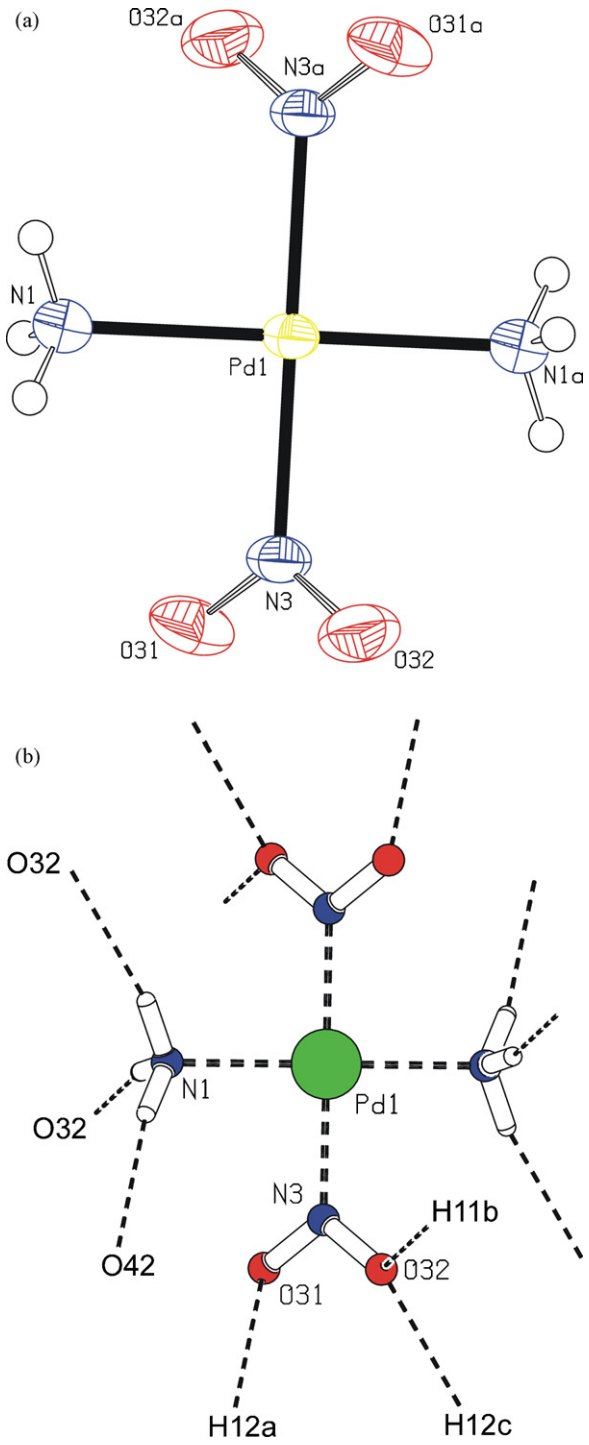

Fig. 2. The complex of **1** (Pd-NN). (a) ORTEP diagram [7,8] at 50% probability level. Half of the molecule is in the asymmetric unit. Atoms labeled with the extension of "a" are symmetry generated. (b) The intermolecular interactions of a complex molecule. All hydrogen bonds are the type of N–H···O.

A block type colourless crystal of **2** was mounted on a loop with oil. Cell parameters were determined by least-squares of the setting angles of all 1704 reflections ($3.57^\circ \leq \theta \leq 27.45^\circ$). Intensity data were collected on a RAXIS-RAPID diffractometer using graphite monochromated MoKα radiation. $R(\sigma) = 0.0496$]. Completeness to $2\theta = 1.000$. Numerical absorption correction was applied.

The initial structure models were found by direct methods using SHELXS97 [4], the anisotropic full-matrix least-squares structure refinements on F^2 were performed by SHELXL97 [5] for all non-

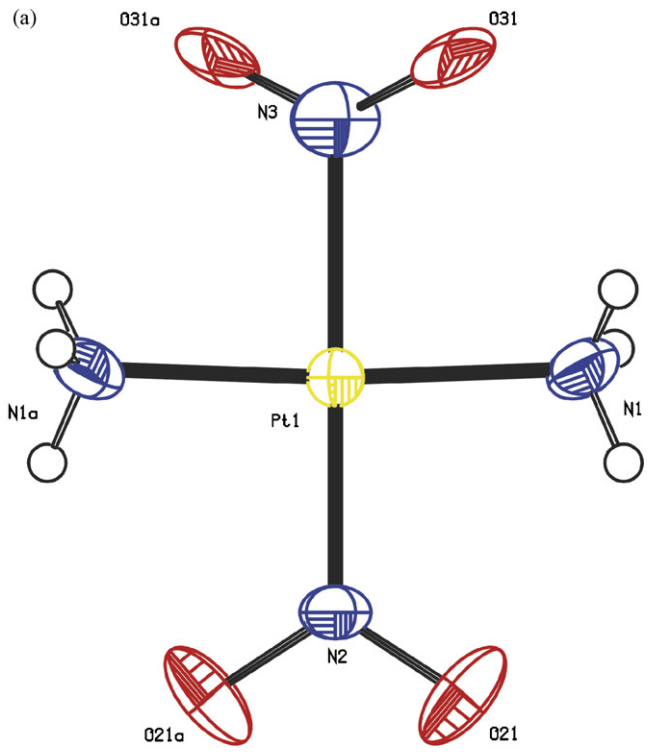

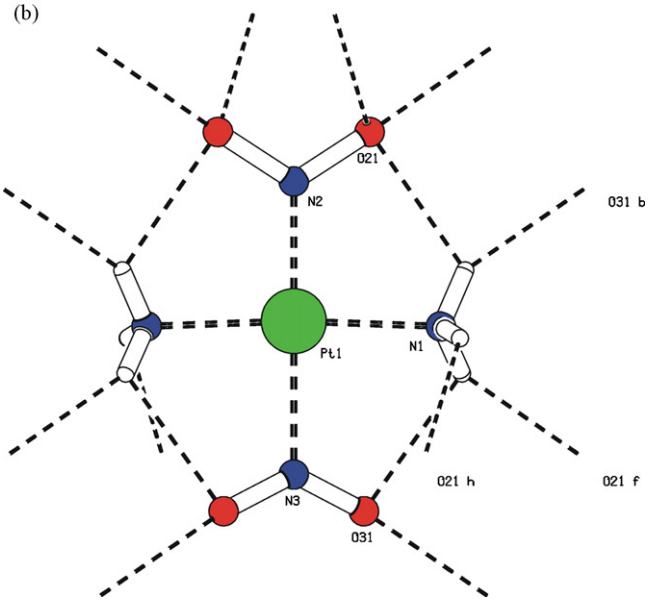

Fig. 3. The complex of **2** (Pt-NN). (a) ORTEP diagram [7,8] at 50% probability level. Half of the molecule is in the asymmetric unit. Atoms labeled with the extension of "a" are symmetry generated. (b) The direction of the intermolecular interactions of a complex molecule. All hydrogen bonds are the type of N–H···O.

hydrogen atoms. The highest peak and deepest hole of the residual electron density synthesis are around the heavy metal centers Pd and Pt cations, respectively.

Hydrogen atomic positions of **1** were calculated from assumed geometries, except H11 that was located in difference maps. Hydrogen atomic positions of **2** were located on difference maps. Hydrogen atoms were included in structure factor calculations but they were not refined. The isotropic displacement parameters of the hydrogen atoms were approximated from the U(eq) value of

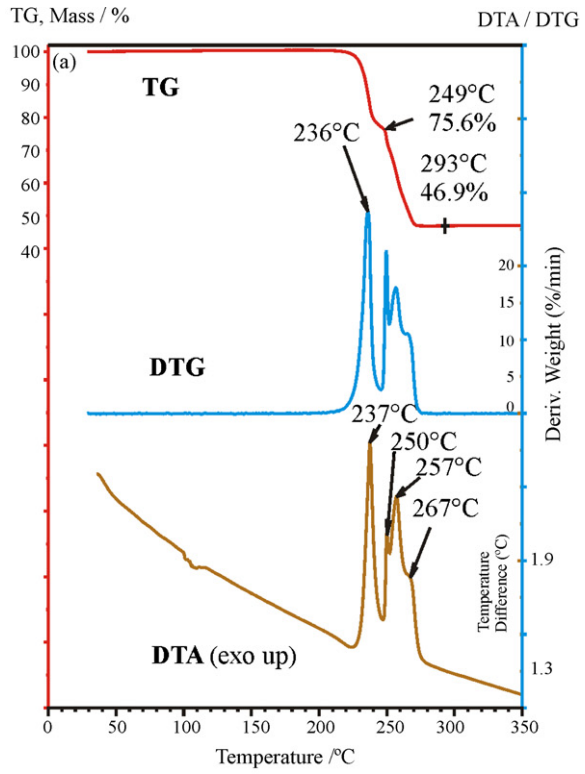

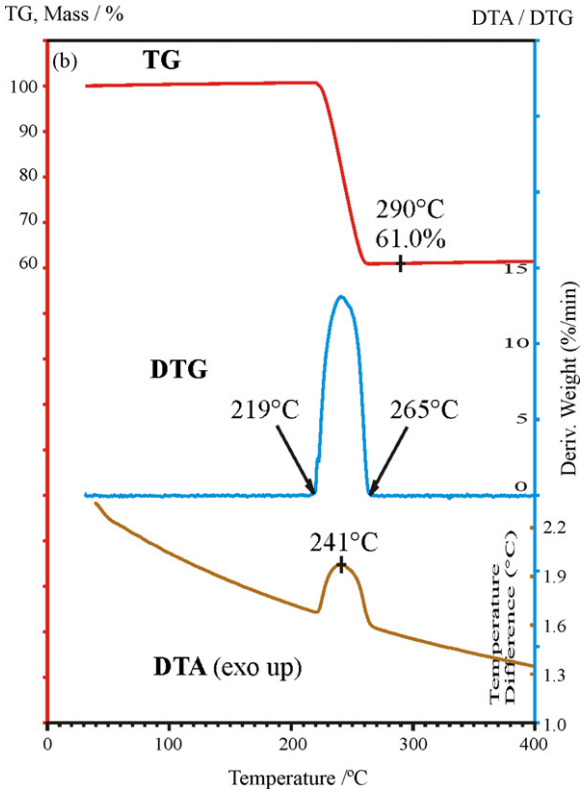

Fig. 4. Simultaneous TG/DTG/DTA curves of (a) crystal **1** (*trans*-$Pd(NH_3)_2(NO_2)_2$) and (b) **2** (*trans*-$Pt(NH_3)_2(NO_2)_2$), measured *in situ* by online coupled TG/DTA–MS system. (He flow 110 mL/min, heating rate 10 °C/min, in sealed Al crucibles with a pinhole on the top, initial masses 3.08 mg and 2.98, respectively).

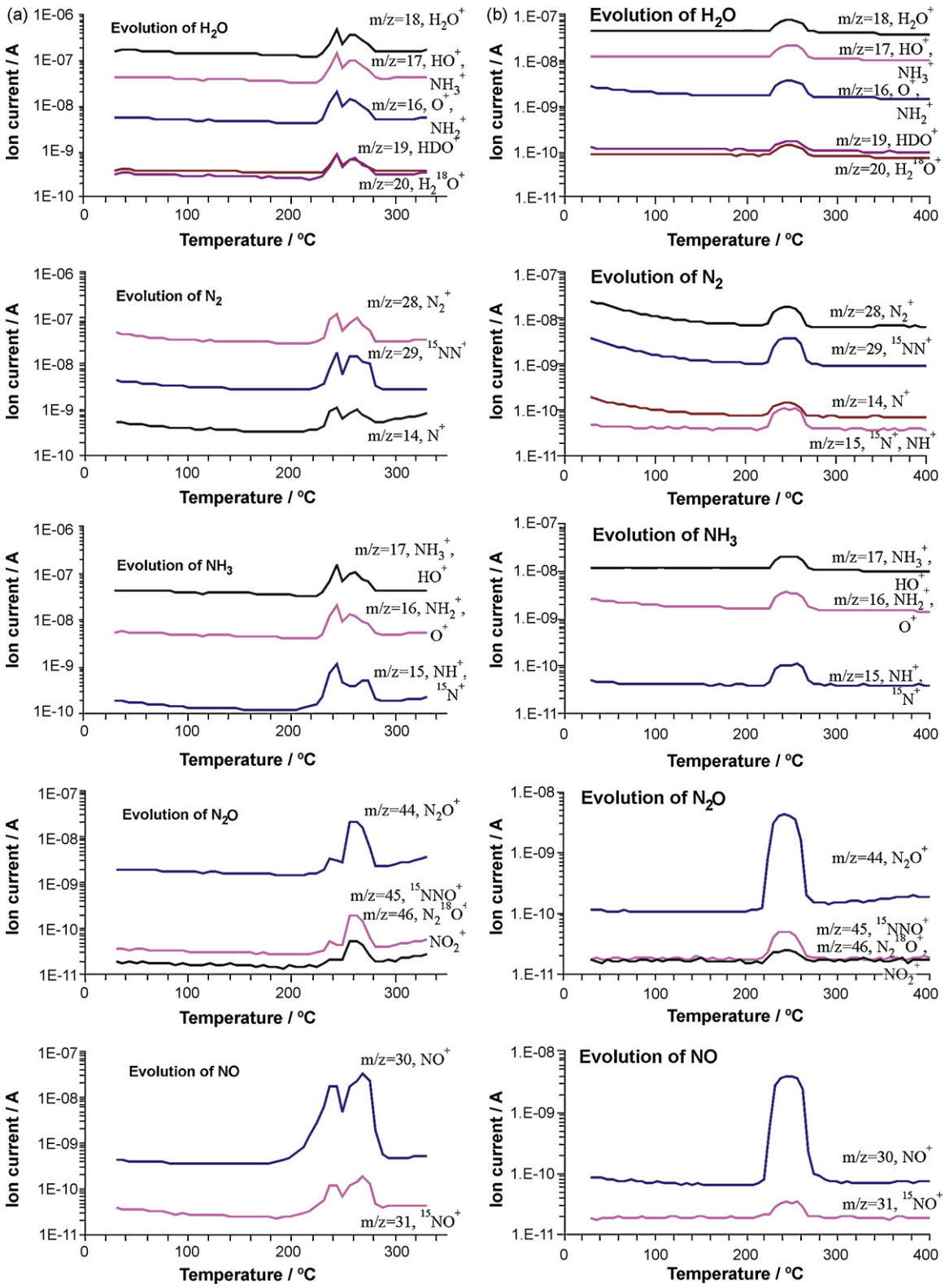

Fig. 5. Gas evolution curves of various of gaseous species, represented by their characteristic mass spectroscopic ion fragments, from (a) crystal **1** (*trans*-$Pd(NH_3)_2(NO_2)_2$) and (b) **2** (*trans*-$Pt(NH_3)_2(NO_2)_2$) in helium, as measured *in situ* by online coupled TG/DTA–EGA–MS system (He flow 110 mL/min, heating rate 10 °C/min, initial mass 3.08 mg and 2.98, respectively).

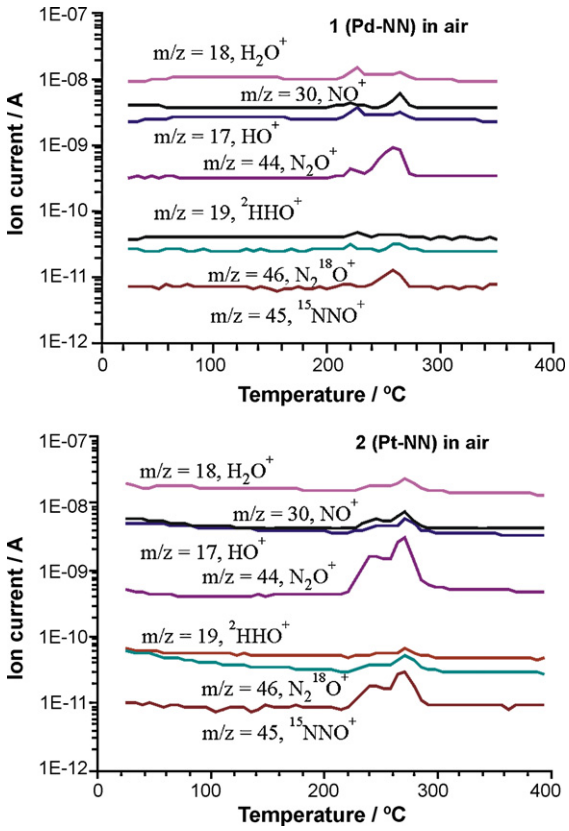

Fig. 6. Gas evolution curves of various of gaseous species, represented by their mass spectroscopic ion fragments, from (a) crystal **1** (*trans*-$Pd(NH_3)_2(NO_2)_2$) and (b) **2** (*trans*-$Pt(NH_3)_2(NO_2)_2$) in air, as measured *in situ* by online coupled TG/DTA–EGA–MS system (He flow 110 mL/min, heating rate 10 °C/min, initial mass 1.46 mg and 2.77, respectively).

the atom they were bonded. Neutral atomic scattering factors were taken from the International Tables for X-ray Crystallography, vol. C [6].

Details of data collection and crystallographic data are presented in Table 1.

2.3. In situ EGA by coupled TG/DTA–MS

A simultaneous TG/DTA apparatus (STD 2960 Simultaneous DTA–TGA, TA Instruments Inc., USA), a heating rate of 10 °C min^{-1}, an air flow rate of 130 mL/min, sample sizes between 2.1 and 8.8 mg, and sealed Al crucibles with a pinhole on the top were used. The mixture of gaseous species could reach a ThermoStar GDS 200 (Balzers Instruments) quadrupole mass spectrometer equipped with Chaneltron detector, through a heated 100% methyl deactivated fused silica capillary tubing kept at $T = 200$ °C. Data collection was carried out with QuadStar 422v60 software in multiple ion detection mode (MID) monitoring 64 selected channels ranging mostly between m/z 12 and 78. Measuring time was ca. 0.5 s for one channel, resulting in time of measuring cycles of ca. 30 s.

2.4. In situ EGA by coupled TG–FTIR

A TGA 2050 thermogravimetric analyzer (TA Instruments, USA) with a heating rate of 10 °C min^{-1}, with air flow rate of 120 mL/min, (and an extra 20 mL/min air as a balance purge) and sample size 1.8–6.5 mg of samples sealed Al crucibles with a pinhole on the top were used. Gaseous species evolved from the sample were led to FTIR gas cell of a BioRad TGA/IR accessory unit equipped with cooled DTGS detector through a heated stainless

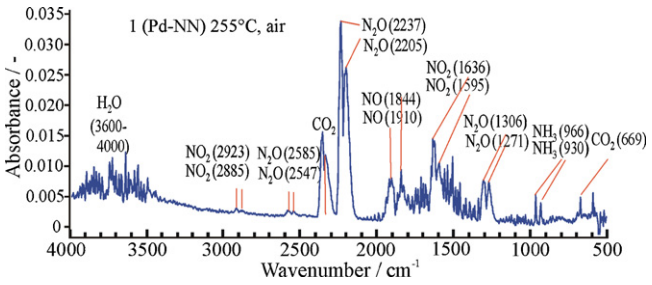

Fig. 7. FTIR spectra of gaseous mixture observed in the air decomposition of **1** (*trans*-$Pd(NH_3)_2(NO_2)_2$) at around 255 °C measured by the online TG–FTIR system (heating rate 10 °C min^{-1}, 130 mL/min air flow, initial mass 3.19 mg).

steal transfer line ($l = 90$ cm, $d_{in} = 2$ mm) kept at $T = 180$ °C. FTIR spectra (550–4000 cm^{-1}) were collected in every 30 s after accumulation of 29 interferograms by a BioRad Excalibur Series FTS 3000 spectrometer using Win IR Pro 2.7 FTIR (BioRad) data collection and evaluation software.

2.5. FTIR spectroscopic and mass spectrometric identification of various gaseous species

The components of released gaseous mixtures were monitored and identified mostly on the basis of their FTIR and MS reference spectra available on world-wide web in the public domain spectral libraries of NIST [9,10].

3. Results and discussion

3.1. FTIR and XRD identification of solid samples **1** (Pd-NN) and **2** (Pt-NN) as trans-$Pd(NH_3)_2(NO_2)_2$ and trans-$Pt(NH_3)_2(NO_2)_2$, respectively

FTIR spectra of samples **1** (Pd-NN) and **2** (Pt-NN) are shown in Fig. 1. The FTIR-spectra of samples **1** (Pd-NN) and **2** (Pt-NN) are similar and resembling to those of *trans*-$Pd(NH_3)_2(NO_2)_2$ and *trans*-$Pt(NH_3)_2(NO_2)_2$, respectively, as far as could be compared in the published wave number range of 400–1400 cm^{-1} [11]. Detailed comparison of the corresponding wave numbers to those of in ref. [11] are given in Table 2. In the range of 1500–1700 cm^{-1} the sample **1** (Pd-NN) shows only one sharp H–N–H bending vibration band at 1647 cm^{-1}, while sample **2** (Pt-NN) displays three sharp ones at 1655(s), 1600(w) and 1558(s) cm^{-1}. It is probably due to the higher complexity of hydrogen bond system in sample **2** (Pt-NN) compared to that of sample **1** (Pd-NN) (see later).

Powder XRD phase identification has confirmed that the XRD pattern of samples **1** (Pd-NN) and **2** (Pt-NN) corroborates with that of unspecified $Pd(NH_3)_2(NO_2)_2$ and *trans*-$Pt(NH_3)_2(NO_2)_2$ (PDF 00-45-598 [12,13] and PDF 00-54-155 [12,14]), respectively. The latter pattern is indexed erroneously in space group *C2/m* (No. 12).

The powder patterns of **1** and **2** reveal the structural differences of the two complexes.

3.2. Molecular and crystal structure of trans-$Pd(NH_3)_2(NO_2)_2$, **1** (Pd-NN) and trans-$Pt(NH_3)_2(NO_2)_2$, **2** (Pt-NN)

The molecular structure, conformation and the complex system of intermolecular interactions of **1** (Pd-NN) and **2** (Pt-NN) were determined by single crystal X-ray diffraction. The complex arrangements are square planar and the configurations are *trans* around the heavy metal (Pd^{2+} or Pt^{2+}) cations surrounded by two ammonia and two nitrite anion as ligands (Figs. 2 and 3). Although the **1** (Pd-NN) and **2** (Pt-NN) are chemically analogue molecules and their configuration is highly similar, their crystals are not isostruc-

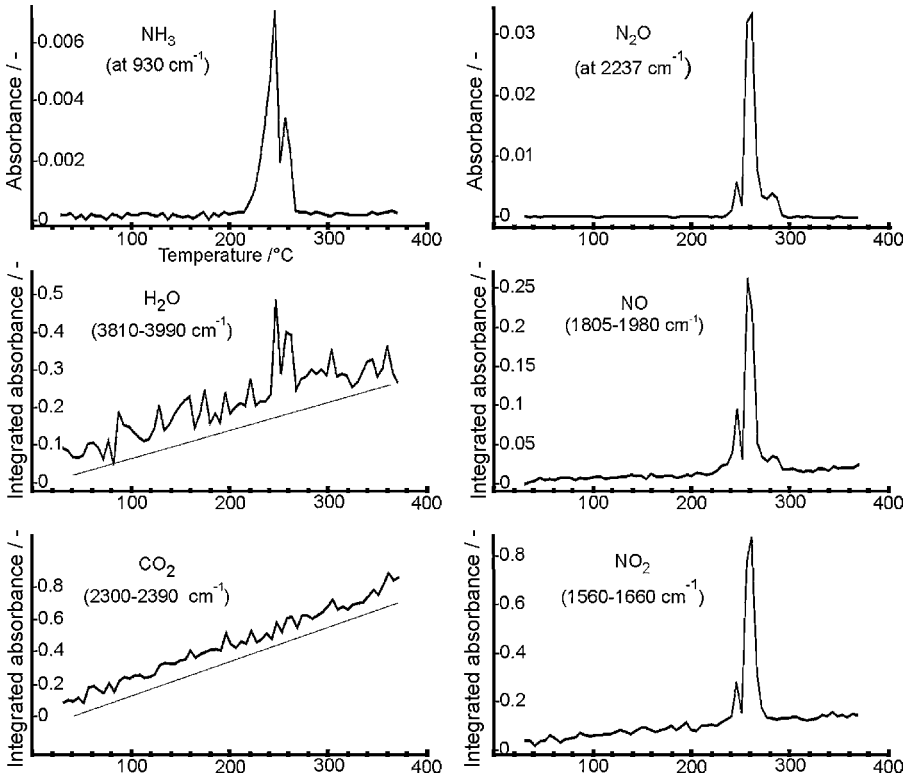

Fig. 8. Evolution courses of gaseous species, from sample **1** (*trans*-$Pd(NH_3)_2(NO_2)_2$),. (by integration of IR-absorbance in their characteristic wave number regions observed in situ TG–EGA–FTIR measurement, 10 °C/min heating rate, 130 mL/min air flow, initial mass 3.19 mg).

tural. While the bright yellow **1** (Pd-NN) crystallizes in triclinic crystal system and *P*-1 space group, the colourless, transparent **2** (Pt-NN) is monoclinic and crystallizes in the space group *C*2. **1** (Pd-NN) complex molecule is organized by the symmetry centre, **2** (Pt-NN) molecule is arranged by a twofold axis along the $N(O_2)PtN(O_2)$ molecular axis. $Z' = 0.5$ in both cases. Cell parameters are given in Table 1. These compounds have not been included yet into the Inorganic Crystal Structure Database (ICSD), [15], although some structural reports have appeared about the Pd complex in Russian [16,17].

Further details of the crystal structure investigations may be obtained from Fachinformationszentrum Karlsruhe, 76344 Eggenstein-Leopoldshafen, Germany (fax: (+49)7247-808-666; e-mail: crysdata@fiz-karlsruhe.de, http://www.fiz-karlsruhe.de/request_for_deposited_data.html) on quoting the ICSD numbers [15]: 420291 for **1** (Pd-NN) and 420292 for **2** (Pt-NN), while figures showing the various crystal packing are available as supplementary material deposited electronically at this journal.

The crystal structures are rich in hydrogen bonds since there are six potential donors and four acceptors in the complexes. All hydrogen bonds are the type of N–H···O (Figs. 2 and 3, Table 3). The main difference of the hydrogen bond systems is, that beyond three 'inter-complex' type hydrogen bonds, complex **2** (Pt-NN) has two additional strong 'intra-complex' type interactions compared to **1** (Pd-NN), what seems mainly to be responsible for the differences in the structural types of crystal lattices. Anyhow, the strong 'intra-complex' type hydrogen bonds are responsible for differences observed in the 1500–1700 cm^{-1} range of FTIR spectra of samples (Fig. 1). The sharp H–N–H bending vibration band at 1647 cm^{-1} in sample **1** (Pd-NN) represents a degenerative vibration mode of N-bonded monodentate NH_3 ligand [18], while sample **2** (Pt-NN) displays split bands at 1655(s), 1600(w) and 1558(s) cm^{-1}, what proves that the occurrence of 'intra-complex' type H-bonds in **2** (Pt-NN) eliminates the degeneration of this vibration mode.

There are six hydrogen bonded rings in the crystal of **1** (Pd-NN) (Table 3, supplementary figure on crystal packing). The $R_4^2(12)$ and $R_4^4(12)$ rings are heterodromic, $R_2^2(10)$ rings are homodromic. The biggest, overlapping $R_4^3(14)$ rings are also heterodromic. The identical rings consist of two N=O and four N–H covalent bonds, four Pd—N coordination bonds and four N-H···O type hydrogen bonds.

All hydrogen bonds in **2** are also the type of N-H···O. They form a three dimensional network in *b* diagonal (Table 3, supplementary figure on crystal packing). In addition to the two intramolecular hydrogen bonds N1-H11···O21 and N1-H12···O31 stabilizing the complex conformation, a two dimensional network is built by N1-H12···O21 and N1-H11···O31 interactions in the *bc* crystallographic plane. The former one is the shortest hydrogen bond, and connects four complex molecules having a heterodromic loop of the type of $R_4^4(18)$, what can be well seen in the packing diagram viewing from the *a* crystallographic axis. Within this ring a smaller loop of $R_4^4(12)$ is formed if we take also the longer N1-H11···O31 interaction into consideration. The planes are connected by N1-H13···O21 hydrogen bonds.

3.3. *Evolution of gaseous species from **1** and **2** in He and air, measured in situ by TG/DTA–EGA–MS and TG–EGA–FTIR spectrometric gas cell system*

The thermogravimetric, as well as its time derivative (DTG), and the DTA curves of crystal **1** (*trans*-$Pd(NH_3)_2(NO_2)_2$) and **2** (*trans*-$Pt(NH_3)_2(NO_2)_2$) are shown in Fig. 4. Both complex **1** and **2** are stable till about 220 °C, when both show an suddenly accelerated decomposition, which is moderated in our cases with application of sealed sample holder with a pinhole on the top. This precaution helps to slow down the violent explosion of the samples and also prevents the solid samples and their residues spewing out of the crucible. The captured residues contain only crystalline phases of metallic Pd (PDF 00-05-681, and Pt (PDF 00-04-802) [12]) according

to our XRD phase analysis. The final amounts of the solid residues of **1** (Pd-NN) and **2** (Pt-NN), 46.92% and 60.97% are close to 45.77% and 60.74%, which are the theoretical mass levels corresponding to metallic palladium and platinum, respectively. Stoichiometric mass level of PdO and PtO would be 52.66% and 65.72%, respectively. Anyhow presence of traces of PdO or PtO [1] cannot be excluded.

Formation of Pt from unspecified $Pt(NH_3)_2(NO_2)_2$ seems to be reported several times in the literature [19–25]. Figueras et al. [19] deposited Pt metal aiming reforming catalysts. Impregnated platinum catalyst, Pt/Al_2O_3 was prepared from such precursor for hydrodechlorination of CCl_4 [20]. As electrocatalysts for direct methanol fuel cells, PtRu/C [21,22] and PtRuRh/C [23] were also obtained from $Pt(NH_3)_2(NO_2)_2$ by thermal reduction. Various oxide-supported Pd metal catalysts were also reported from unspecified $Pd(NH_3)_2(NO_2)_2$ by impregnation methods (on SnO_2, ZrO_2, CeO_2 [24], or on SiO_2 [25,26]. Even effect of noble metals (Pt or Pd coming from the above precursors) on VOCs (aromatic volatile organic carbons) sensing properties of WO_3 thin film sensors were also studied [27].

Kinoshita et al. [28] studied the thermal stability of platinum diamino dinitrite ($Pt(NH_3)_2(NO_2)_2$) for preparation Pt catalyst in flowing hydrogen, argon, air, oxygen, and vacuum by thermogravimetry (TG), and separately in air, argon, and hydrogen by DTA, in open crucibles, at about 10 mg of initial mass. The thermal decomposition of $Pt(NH_3)_2(NO_2)_2$ had occurred with a rapid, violent weight loss at well defined temperatures depending on the surrounding gas environment, at 127, 208, 230, 232, and 180 °C in hydrogen, argon, air, oxygen, and vacuum, respectively [28]. Exothermic heat effect escorted the decomposition even in air, argon, and hydrogen, although poor agreement was observed for the onset temperatures of thermal decomposition in the separate TG and DTA apparatuses [28]. Hernandez and Choren studied also the thermal decomposition of diammineplatinum(II) nitrit ($Pt(NH_3)_2(NO_2)_2$) in oxygen, helium and hydrogen observing single step decomposition at temperatures 240, 240, and 125 °C, respectively, accompanied by highly exothermic effects in all atmospheres, while the solid products of transformation was calculated to be Pt according to TG diagrams [29] in all the cases.

In our simultaneous TG/DTA experiments of **1** (Pd-NN), the single pinhole has usually become probably temporary closed by some solid particles of sample, resulting in delayed and varied dynamics and in some more virtual stages of decomposition shown by both TG, DTG, and DTA curves, compared to the smooth changes in case of **2** (Pt-NN) cf. Fig. 4a and b.

The evolution courses of individual gaseous products of decomposing crystal **1** (*trans*-$Pd(NH_3)_2(NO_2)_2$) and **2** (*trans*-$Pt(NH_3)_2(NO_2)_2$), as identified and monitored by TG/DTA–EGA–MS in He are shown in Fig. 5. The ion fragments, which suffered changes, indicate (at least, do not exclude) the evolution of N_2, H_2O, NH_3, N_2O, and NO gases during the decomposition, what follows the overall dynamics of mass losses represented by the DTG curves.

The TG/DTA–EGA–MS experiments carried out in air (Fig. 6) for **1** (*trans*-$Pd(NH_3)_2(NO_2)_2$) and **2** (*trans*-$Pt(NH_3)_2(NO_2)_2$) could only confirm evolution of H_2O, N_2O and NO in both cases, but the MS system was not able to detect of N_2 and NH_3, because of the vast presence of nitrogen originating from the flowing air and providing high lever of background and background noises.

According to Figueras et al. [19] $Pt(NH_3)_2(NO_2)_2$ decomposes under vacuum into nitrogen and water, unfortunately neither experimental proof nor source of reference was given on the chemical identity of evolved gases.

In order to check the identity of the evolved gases, comparatively TG–EGA–FTIR gas cell measuring system has also been applied. In air, the evolution of the various gases (H_2O, NH_3, N_2O, and NO, except N_2, which is not detectable by FTIR) is confirmed in case of **1** (*trans*-$Pd(NH_3)_2(NO_2)_2$) by the FTIR-spectra, as well (Fig. 7). In addition, evolution of NO_2, nitrogen dioxide has also definitely been observed in air (See Fig. 7). This gas could not be conclusively detected by EGA–MS.

The evolution patterns of the individual gas components are presented in Fig. 8. The time shift of H_2O and CO_2 signals is not part of the degradation processes. Probably, initially NH_3 forms from crystal **1** (Pd-NN), whose oxidation into N_2O, NO and NO_2 are catalyzed by the metallic Pd particles.

4. Summary and conclusion

We have successfully crystallized from the impregnation solutions, the crystals of analogous **1** (*trans*-$Pd(NH_3)_2(NO_2)_2$), and **2** (*trans*-$Pd(NH_3)_2(NO_2)_2$), respectively. The molecular and crystal structures have been determined by single crystal X-ray diffraction, and their thermal stability has also been studied. The chemically and configurationally analogous compounds crystallized in different crystal systems and space groups having also different network of intermolecular interactions. They are both stable till ca. 220 °C, when they suddenly decompose both in inert (He) and in oxidizing (air) atmosphere. We have also been able to capture the spewing residues of thermal decomposition in a sealed Al crucible with a pinhole on the top used in simultaneous TG/DTA experiments. Despite former XPS findings [1] the amount of residues and their powder X-ray diffraction phase analysis shows single step and stoichiometric formation of metallic palladium and platinum, respectively. Thermal degradation of a $[Pt(NH_3)_5OH]Cl_3.H_2O$ salt [30] in oxygen produced PtO_2 as an intermediate before the formation of Pt above 430 °C, but it is not happened in our case.

In situ evolved gas analysis of the released gas mixture from decomposition of both compounds indicated and monitored the formation of N_2, H_2O, NH_3, N_2O, and NO gases as gaseous product components (even presence of NO_2 could not be excluded) by TG/DTA–EGA–MS in He purge atmosphere, while TG–EGA–FTIR spectroscopy in air has also proven the elaboration of H_2O, NH_3, N_2O, NO and NO_2, (unfortunately N_2 is not IR active and not detectable by FTIR). Beyond water and nitrogen formation [18], the occurrence of ammonia and various nitrogen oxides represent a more sophisticated degradation mechanism of the compounds, which seems to be not too much influenced neither by the inertness nor oxidative nature of atmosphere used for the thermal decomposition, or by the different H-bonding system of the two complexes.

The intense and violent exothermic gas evolution from these solid complexes **1** and **2** at about 220 °C makes them probably sensitive to shock, what needs to be essentially beware in mind during a scaling up of sensor fabrication.

Acknowledgements

P.B. and M.C. acknowledge the National Science and Technology Office for an X-ray diffractometer purchase grant (MU-00338/2003). J.M. and G.P. also thanks for the purchase grant of a new HT-XRD apparatus supported by the EU and Hungarian government (GVOP-3.2.1.-2004-04-0224, KMA).

Appendix A. Supplementary data

Supplementary data associated with this article can be found, in the online version, at doi:10.1016/j.tca.2009.02.006.

References

[1] G. Kiss, V.K. Josepovits, K. Kovács, B. Ostrick, M. Fleischer, H. Meixner, F. Réti, Thin Solid Films 436 (2003) 115–118.

[2] K. Harms, XCAD4 Data Reduction Program for CAD4 Diffractometers, Philipps-Universität Marburg, Germany, 1996.
[3] A.C. North, D.C. Philips, F. Mathews, Acta Cryst. A24 (1968) 350–359.
[4] G.M. Sheldrick, SHELXS-97 Program for Crystal Structure Solution, University of Göttingen, Germany, 1997.
[5] G.M. Sheldrick, SHELXL-97 Program for Crystal Structure Refinement, University of Göttingen, Germany, 1997.
[6] International Tables for X-ray Crystallography Vol. C., in: A.J.C. Wilson (Ed.), Kluwer Academic Publishers, Dordrecht, Tables 6.1.1.4 (pp. 500–502), 4.2.6.8 (pp. 219–222) and 4.2.4.2 (pp. 193–199), 1992.
[7] A.L. Spek, Acta Cryst. A46, C-34, Windows implementation by L.J. Farrugia, (1998), Department of Chemistry, University of Glasgow, UK, 1990.
[8] M.N. Burnett, C.K. Johnson, ORTEP-III, ORNL Report 6895, Windows implementation by, L.J. Farrugia (1998), Department of Chemistry, University of Glasgow, UK, 1996.
[9] NIST Chemistry Webbook Standard Reference Database No. 69, June 2005 Release (http://webbook.nist.gov/chemistry).
[10] Spectral Database for Organic Compounds, SDBS, National Institute of Advanced Industrial Science and Technology, Japan, http://riodb01.ibase.aist.go.jp/sdbs/cgi-bin/direct_frame_top.cgi.
[11] M. Le Postollec, J.-P. Mathieu, H. Poulet, J. Chim. Phys. Phys. Chim. Biol. 60 (1963) 1319–1333 (Fr.) CA 60:57358.
[12] International Centre for Diffraction Data (ICDD), Powder Diffraction File (PDF), PDF-2 Release, 2007.
[13] S. Kirik, I. Yakimov, A. Blohkin, L. Soloyov, Institute of Chemistry, Academy of Science, Krasnoyarsk, Russia, ICDD Grant-in-Aid, 1994.
[14] S. Kirik, L. Solovyov, A. Blohkin, R. Mulagaleev, Institute Of Chemistry, Academy of Science, Krasnoyarsk, Russia, ICDD Grant-in-Aid.(2002).
[15] Inorganic Crystal Structure Database (ICSD), Fachinformationszentrum Karlsruhe (FIZ) and National Institute of Standards and Technology (NIST), Version Release 2008/2.
[16] S.A. Gromilov, S.P. Khranenko, V.I. Alekseev, I.A. Baidina, A.V. Belyaev, Zh. Neorgan. Khim. 43 (1998) 427–429 (Russ.), CA 129:10928.
[17] A.I. Blokhin, L.A. Solov'ev, M.L. Blokhina, I.S. Yakimov, S.D. Kirik, Russ. J. Coord. Chem. (Transl. Koordinatsionnaya Khimiya) 22 (1996) 185–189, CA 124: 275020.
[18] K. Nakamoto, Infrared and Raman Spectra of Inorganic and Coordination Compounds, Wiley-Interscience, 1986.
[19] F. Figureas, B. Mencier, L. de Mourgues, C. Naccache, Y. Trambouze, J. Catal. 19 (1970) 315–321.
[20] T. Kawaguchi, Y. Rachi, W. Sugimoto, Y. Murakami, Y. Takasu, J. Appl. Electrochem. 36 (2006) 1117–1125.
[21] Z.B. Wang, G.P. Yin, P.F. Shi, J. Power Sources 163 (2007) 688–694.
[22] Z.B. Wang, G.P. Yin, P.F. Shi, J. Electrochem. Soc. 152 (2005) A2406–A2412.
[23] J.W. Bae, I.G. Kim, J.S. Lee, K.H. Lee, E.J. Jang, Appl. Catal. A: Gen. 240 (2003) 129–142.
[24] T. Mitsui, K. Tsutsui, T. Matsui, R. Kikuchi, K. Eguchi, Appl. Catal. B: Environ. 78 (2008) 158–165.
[25] J. Sakauchi, H. Sakagami, N. Takahashi, T. Matsuda, Y. Imizu, Catal. Lett. 99 (2005) 257–261.
[26] K. Ito, M. Ohshima, H. Kurokawa, K. Sugiyama, H. Miura, Catal. Commun. 3 (2002) 527–531.
[27] K. Kanematsu, J. Tamaki, S. Kajita, Chem. Sensors 23 (Suppl. B) (2007) 34–36.
[28] K. Kinoshita, K. Routsis, J.A.S. Bett, Thermochim. Acta 10 (1974) 109–117.
[29] J.O. Hernández, E.A. Choren, Thermochim. Acta 71 (1983) 265–272.
[30] H. Hokkanen, T. Leskelä, L. Niinistö, H.A. Laitinen, Thermochim. Acta 191 (1991) 35–40.